Adaptive Speed Observer for a Stand-alone Doubly Fed Induction Generator Feeding Nonlinear and Unbalanced Loads

M. Pattnaik, *Student Member, IEEE* and D. Kastha, *Member, IEEE*

***Abstract*— In this paper an improved sensorless control algorithm for a Variable Speed Constant Frequency (VSCF) doubly fed induction generator is presented. Unlike previously reported methods the proposed algorithm does not require the rotor position or speed information for the stator field orientation of the rotor variables. The slip frequency is estimated by a reactive power based model reference adaptive observer and is used in the rotor current controllers for back-emf compensation. A new on-line estimation method for the magnetizing inductance of the machine is also proposed to enhance the performance of the controller. Small signal models of the slip frequency and the magnetizing inductance estimators are developed to aid their design. The proposed algorithm is capable of 'speed catching on the fly' and performs satisfactorily with balanced, unbalanced, linear and nonlinear loads (in any combination) particularly, nonlinear unbalanced loads, which has not been reported in literature so far. Experimental and simulation results are presented to demonstrate excellent load voltage regulation property of the control algorithm during severe transient operating conditions. Total Harmonic Distortion and unbalance of the load voltage and stator current even with large nonlinear/ unbalanced loads are also found to be much smaller compared to systems reported earlier.**

***Index Terms*— Doubly Fed Induction Generator, Model Reference Adaptive System (MRAS), stand-alone VSCF generator, sensorless control, wind energy.**

I. NOMENCLATURE

General

v_{ds}^s, v_{qs}^s : *d*, *q*-axis stator voltage in the stationary ref. frame.

i_{ds}^s, i_{qs}^s : *d*, *q*-axis stator current in the stationary ref. frame.

$\lambda_{ds}^s, \lambda_{qs}^s$: *d*, *q*-axis stator flux in the stationary ref. frame.

v_{dr}^r, v_{qr}^r : *d*, *q*-axis rotor voltage in the rotor ref. frame.

i_{dr}^r, i_{qr}^r : *d*, *q*-axis rotor current in the rotor ref. frame.

Q_{ref}, Q_{est}: Instantaneous and steady state rotor reactive power

$r_s, r_r^{'}$: Per phase stator and rotor resistances (stator referred).

$l_s, l_r^{'}$: Per phase stator, rotor self inductances (stator referred).

l_m : Per phase magnetizing inductance.

σ : Total leakage coefficient.

l_f, r_f : Filter inductance and internal resistance.

C, c_f : DC link and filter capacitance.

ω_e : Rotational speed of the stator flux(elect. rad/sec).

ω_r : Rotor speed of the induction machine(elect. rad/sec).

ω_{sl} : Slip frequency(elect. rad/sec).

Superscripts

^ : Estimated value.

* : Reference value.

M. Pattnaik is with the Department of Electrical Engineering, National Institute of Technology, Rourkela 769008, India (e-mail: monalisa.pattnaik@gmail.com).

D. Kastha is with the Department of Electrical Engineering, Indian Institute of Technology, Kharagpur 721302, India (e-mail: kastha@ee.iitkgp.ernet.in).

II. INTRODUCTION

DOUBLY Fed Induction Generators (DFIG) are widely used with variable speed wind turbines for electrical power generation. The operation and control of grid connected DFIG based systems [1] – [4] are well established. In recent years, research on stand-alone mode of operation of such generators has gained considerable attention.

The design and performance of a DFIG based stand-alone VSCF generating system has been presented for wind power application in [5]. The algorithm requires a speed sensor and only linear balanced load was considered. Speed sensorless control is highly desirable for DFIG as encoder failure is one of the most significant failure modes of these systems. Moreover, in a stand-alone application, balanced loading condition of the generator cannot always be guaranteed. Also, with the proliferation of consumer electronic devices a substantial portion of the load current can be expected to be non-linear. Any stand-alone generation system must address these issues. Several model reference adaptive rotor speed observers are proposed in [6], [7] for stand-alone DFIG but has not been tested with nonlinear and unbalanced loads. In [8], [9] a direct voltage control method is used for speed sensorless control of a stand-alone induction generator. However, it cannot decouple voltage magnitude and frequency control loops. No design methodology for these controllers are presented either which makes prediction regarding performance/ stability difficult. Resistive load transient produced significant disturbance in the stator terminal voltage as shown in the paper. A sensorless control scheme for the stand-alone DFIG, proposed in [10], also suffers from undesirable transients in the load terminal voltage during load change. The speed range of operation (±10% around synchronous speed) is also rather restricted. The proposed scheme incorporates active filtering function in the stator side converter to handle nonlinear loads. However, the reported harmonic compensation performance is not very good.

Unbalanced loads are not considered in this paper. The control system discussed in [11] for DFIG supplying unbalanced loads, also uses the stator side converter for unbalance compensation. But, performance of the system with nonlinear loads has not been reported in this paper. Results with sensorless algorithm are not presented either. The sensorless stator flux oriented control scheme for slip ring induction machines presented in [12] is rotor resistance dependant. But, this parameter is not estimated. MRAS based sensorless control methods for DFIG have also been proposed in [13], [14]. However, as discussed by the authors, the performance of the method degrades at light load when the value of the magnetizing inductance used in the controller differs from the actual machine parameter. Also the algorithm is very sensitive to measurement offsets in the rotor current. Another sensorless rotor position estimator based on torque calculation, proposed in [15], also suffers from similar problems as in [13] & [14]. In addition this algorithm exhibits an unstable region in the rotor current plane which must be avoided during operation. Unbalance and harmonic load compensation techniques proposed in [16]-[18] for the stand-alone DFIG uses the rotor side converter for harmonic current injection. Consequently, they suffer from the disadvantages of harmonic heating of the machine and pulsating torques as acknowledged by the authors themselves. Moreover, the proposed algorithms use speed sensors which compromises system reliability. Reference [19] presents a reactive power based and a stator flux based MRAS speed estimation techniques for DFIM drives. In [20], a sensorless speed estimation technique for DFIM using rotor reactive power based MRAS observer is proposed. The proposed reactive power based MRAS algorithms are shown to be independent of any variation in stator and rotor resistances. However, neither of them discusses the effect of variation of the self and the mutual inductance on the rotor speed estimation. While the stator flux based MRAS proposed in [19] is claimed to be independent of stator resistance variation, the effect of rotor resistance variation on this algorithm is not studied.

A comparative evaluation of stator flux and rotor current based MRAS speed observers presented in [21] establishes that these algorithms cannot be used during DC link voltage build up phase of the stand-alone DFIG since the estimator start-up transient affects the voltage build up process. This problem is overcome in [23] by using a reactive power based MRAS observer for the rotor slip frequency in the DFIG based stand-alone generation system reported in [22]. The proposed algorithm does not require the rotor position or speed information for the stator field orientation of the rotor variables. The rotor current control loops uses the estimated slip speed for back-emf compensation. Since the rotor flux linkage is relatively small during the DC link voltage build up phase the starting transient of the slip estimator does not affect the rotor current control performance. Simulation results presented in [23] establishes that the excellent load voltage regulation property of the original speed sensor based system [22] are retained by this algorithm. However, the algorithm presented in [23] is dependent on the value of the mutual inductance. Therefore, an estimation technique for this parameter is presented in this paper. In addition, small signal models for both the mutual inductance estimator and the slip frequency estimator are presented. The performance of the control scheme is validated through experimental and simulation results under different transient conditions like, speed, direct-axis rotor current and load variation. Organisation of the paper is given below. Section III presents sensorless control strategy for the DFIG base VSCF system. Modelling and design of the estimators are discussed in section IV. Section V presents the experimental and simulation results which establish excellent performance of the proposed algorithm during severe transient operating conditions and unbalanced/ harmonic loading conditions. Finally conclusions are drawn in section VI.

III. SENSORLESS CONTROL OF THE DFIG BASED STAND-ALONE VSCF GENERATOR

The basic operation and control of the stand-alone DFIG based generation system shown in Fig.1 is described in detail in [22]. Converter – II in Fig. 1 controls the load terminal voltage in a closed loop manner to emulate a constant voltage constant frequency grid. Converter-I maintains a constant DC link voltage by adjusting the mechanical power input to the machine through the torque producing component of the rotor current. The flux producing component of the rotor current is used to control the stator side power factor of the machine.

A speed sensorless control algorithm for this system is proposed in [23]. It does not require the rotor position information for reference frame conversions but uses the slip speed information estimated by a reactive power based MRAS (Q-MRAS) observer for the back-emf compensation in the rotor current controllers. Fig. 2 shows the complete block diagram of the control system. As this controller has been discussed in detail in [22] & [23]. Only a brief overview is presented here, for the sake of completeness.

The stator field oriented reference frame is used for controller development. Eqns.(1) & (2) computes the stator flux linkage and the unit vectors for field orientation.

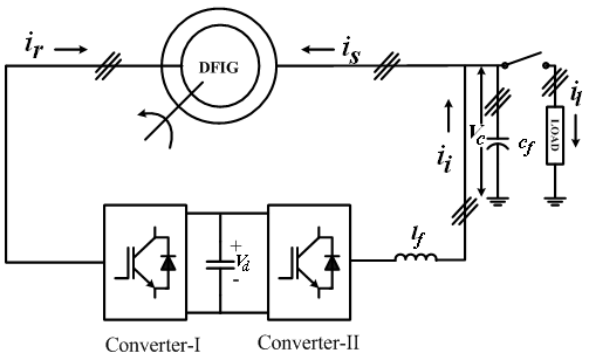

Fig. 1. Schematic diagram of a stand-alone DFIG based VSCF system.

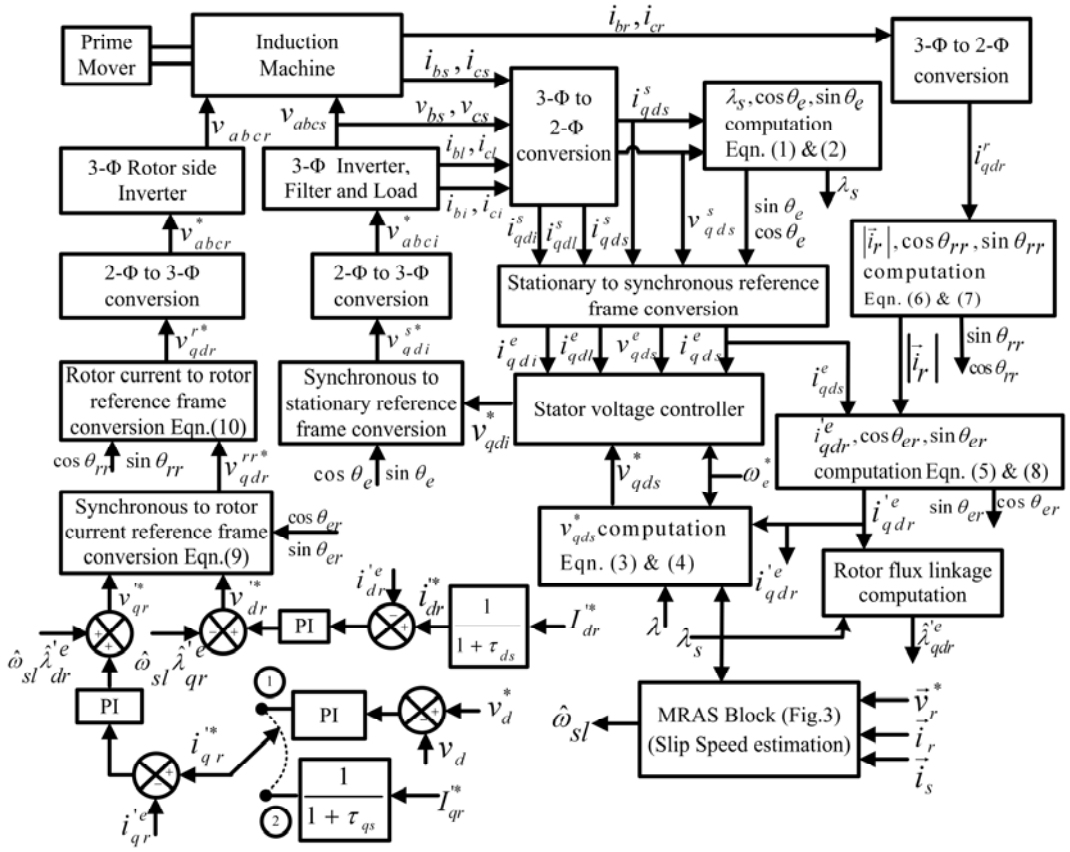

Fig.2. Control block diagram for the proposed sensorless generation system.

$$\lambda_{ds}^{s} = \int \left(v_{ds}^{s} - r_s i_{ds}^{s} \right) dt;\ \lambda_{qs}^{s} = \int \left(v_{qs}^{s} - r_s i_{qs}^{s} \right) dt; \quad (1)$$

$$\lambda_s = \sqrt{(\lambda_{ds}^{s})^2 + (\lambda_{qs}^{s})^2};\ \cos\theta_e = \frac{\lambda_{ds}^{s}}{\lambda_s};\ \sin\theta_e = \frac{\lambda_{qs}^{s}}{\lambda_s}; \quad (2)$$

The machine stator voltage components (v_{qs}^{e} & v_{ds}^{e}) are closed loop controlled to follow the following references.

$$v_{ds}^{e*} = \frac{\lambda}{\tau_s} - \frac{l_m}{\tau_s} i_{dr}^{'e};\ \text{where, } \tau_s = \frac{l_s}{r_s} \quad (3)$$

$$v_{qs}^{e*} = \omega_e^{*} \lambda_s - \frac{l_m}{\tau_s} i_{qr}^{'e} \quad (4)$$

It can be easily shown that v_{qs}^{e} & v_{ds}^{e} following their respective references will regulate the magnitude of stator flux linkage (λ_s) and the stator frequency (ω_e) to their desired values λ and ω_e^{*} respectively. The closed loop controllers for the stator voltages follow a cascade structure with inner filter current (current through 'l_f' in Fig. 1) control loops. References for the filter current control loops are obtained by adding the outputs of the outer voltage control loops with the respective load and stator current components. Bandwidth of these current control loops largely determines the harmonic/unbalance compensation performance of the system as has been discussed in detail in [22]. To obtain the feedback values of the rotor current components (i_{qr}^{e} & i_{dr}^{e}) for the rotor current controllers in Fig. 2 as well as to transform the commanded rotor voltages (v_{qr}^{e*} & v_{dr}^{e*}) to the rotor reference frame, in the absence of a rotor position sensor, the following procedure is proposed in [23]. i_{qr}^{e} & i_{dr}^{e} in the stator flux oriented reference frame are given by:

$$i_{qr}^{e} = -\frac{l_s}{l_m} i_{qs}^{e};\ i_{dr}^{e} = \sqrt{\left(|\vec{I}_r| \right)^2 - \left(i_{qr}^{e} \right)^2} \quad (5)$$

Rotor current vector magnitude ($|\vec{I}_r|$) and its angle with respect to the rotor reference frame are:

$$|\vec{I}_r| = \sqrt{\left(i_{dr}^{r} \right)^2 + \left(i_{qr}^{r} \right)^2} \quad (6)$$

$$\cos\theta_{rr} = \frac{i_{dr}^{r}}{|\vec{I}_r|};\ \sin\theta_{rr} = \frac{i_{qr}^{r}}{|\vec{I}_r|} \quad (7)$$

The angle of the *d*-axis of the rotor current oriented reference frame with respect to the *d*-axis of the stator flux oriented reference frame (θ_{er}) is computed from

$$\cos\theta_{er} = \frac{i_{dr}^{e}}{|\vec{I}_r|};\ \sin\theta_{er} = \frac{i_{qr}^{e}}{|\vec{I}_r|} \quad (8)$$

Equation (9) given below transforms the rotor voltage commands v_{qr}^{e*} & v_{dr}^{e*} from the synchronously rotating reference to the rotor current oriented reference frame.

$v_{qr}^{rr*} = v_{qr}^{e*}\cos\theta_{er} - v_{dr}^{e*}\sin\theta_{er};\ \ v_{dr}^{rr*} = v_{qr}^{e*}\sin\theta_{er} + v_{dr}^{e*}\cos\theta_{er}$ (9)

v_{qr}^{rr*} and v_{dr}^{rr*} are then transformed directly to the rotor reference frame using equation (10).

$v_{qr}^{r*} = v_{qr}^{rr*}\cos\theta_{rr} + v_{dr}^{rr*}\sin\theta_{rr};\ \ v_{dr}^{r*} = -v_{qr}^{rr*}\sin\theta_{rr} + v_{dr}^{rr*}\cos\theta_{rr}$ (10)

These conversions do not require the rotor position information. Only the slip speed information is used by the rotor current controllers for back-emf compensation as shown in Fig.2. This slip speed is estimated by a reactive power based MRAS (Q-MRAS) observer as described next.

A. Reactive Power Based MRAS Observer

The implementation of Q-MRAS is shown in Fig.3. The rotor voltage equations in the stator flux oriented reference frame are given by:

$$v_{dr}^{*e} = r_r' i_{dr}^{'e} - \omega_{sl}\lambda_{qr}^{'e} + p\lambda_{dr}^{'e} \quad (11)$$

$$v_{qr}^{*e} = r_r' i_{qr}^{'e} + \omega_{sl}\lambda_{dr}^{'e} + p\lambda_{qr}^{'e} \quad (12)$$

The expression of instantaneous reactive power (IRP) in the rotor reference frame is

$$Q_{ref} = \vec{v}_r \otimes \vec{i}_r = v_{qr}^r i_{dr}^r - v_{dr}^r i_{qr}^r \quad (13)$$

In the equation above (as well as in Fig. 3) the symbol '$\otimes$' indicates "cross product" between two vectors. Q_{ref} can be approximated assuming that v_{dr}^r and v_{qr}^r exactly follow the reference signals v_{dr}^* and v_{qr}^*. So, (13) can be expressed as

$$Q_{ref} = v_{qr}^{*r} i_{dr}^r - v_{dr}^{*r} i_{qr}^r \quad (14)$$

The expression of Q_{est} at steady state, obtained by applying the condition of stator flux orientation and simplifying, is:

$$Q_{est} = \hat{\omega}_{sl}\left[\sigma l_r I_r^2 + \frac{l_m}{l_s}\lambda_s i_{dr}^{'e}\right] \quad (15)$$

It is seen that Q_{est} is independent of the rotor resistance.

The MRAS error is given by: $\varepsilon = Q_{ref} - Q_{est}$ (16)

The input to the adaptation mechanism (a PI controller) is this error (ε) and the output is the estimated slip speed ($\hat{\omega}_{sl}$).

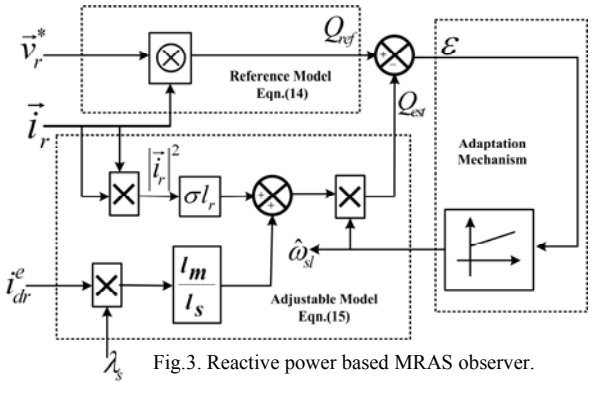

Fig.3. Reactive power based MRAS observer.

This $\hat{\omega}_{sl}$ tunes the adjustable model to drive the error to zero.

IV. SMALL SIGNAL MODELLING OF THE ESTIMATORS

In the previous section equation (5), was used to estimate i_{qr}^e & i_{dr}^e from the corresponding components of the stator currents. This estimate, however is dependent on the machine parameters l_m and l_s. In actual operation l_m may vary substantially depending on the magnetizing flux of the machine. Therefore, a method for on line estimation of l_m is presented in this section. Once l_m is correctly estimated l_s is found by using the relation $l_s = l_m + l_{ls}$. In this work l_{ls} is assumed to remain constant.

Defining $k_m = \frac{1}{l_m}$ equation (5) can be rewritten as

$$\hat{i}_{qr}^e = -\left(1 + \hat{k}_m l_{ls}\right) i_{qs}^e \quad (17)$$

$$\hat{i}_{dr}^e = \sqrt{\left|I_r^2\right| - \hat{i}_{qr}^{e\,2}} \quad (18)$$

In the above equations a variable / parameter with a '^' denotes the estimate of the variable / parameter.

$$\hat{i}_{qr}^e - i_{qr}^e = \left(k_m - \hat{k}_m\right) l_{ls} i_{qs}^e \quad (19)$$

$$\hat{i}_{dr}^{e\,2} = i_r^2 - \hat{i}_{qr}^{e\,2} \quad (20)$$

Assuming $\left(\hat{i}_{dr}^e - i_{dr}^e\right) << i_{dr}^e$ and $\left(\hat{i}_{qr}^e - i_{qr}^e\right) << i_{qr}^e$

$$\hat{i}_{dr}^e - i_{dr}^e = -\frac{i_{qr}^e}{i_{dr}^e}\left(\hat{i}_{qr}^e - i_{qr}^e\right) = l_{ls}\frac{i_{qr}^e}{i_{dr}^e} i_{qs}^e\left(\hat{k}_m - k_m\right) \quad (21)$$

Another estimate of i_{dr}^e is obtained from the equation

$$\tilde{i}_{dr}^e = \hat{k}_m\left(\lambda_s - l_{ls} i_{ds}^e\right) - i_{ds}^e \quad (22)$$

$$\tilde{i}_{dr}^e - i_{dr}^e = \left(\hat{k}_m - k_m\right)\left(\lambda_s - l_{ls} i_{ds}^e\right) \quad (23)$$

$$\tilde{i}_{dr}^e - i_{dr}^e = \left[\lambda_s - l_{ls}\frac{i_{qs}^e i_{qr}^e + i_{ds}^e i_{dr}^e}{i_{dr}^e}\right]\left(\hat{k}_m - k_m\right) \quad (24)$$

Now,

$$i_{qs}^e = -\frac{i_{qr}^e}{1 + k_m l_{ls}} \quad \text{and} \quad i_{ds}^e = \frac{k_m\lambda_s}{1 + k_m l_{ls}} - \frac{i_{dr}^e}{1 + k_m l_{ls}} \quad (25)$$

$$\therefore \tilde{i}_{dr}^e - \hat{i}_{dr}^e = \left[\frac{\lambda_s}{1 + k_m l_{ls}} + \frac{l_{ls}}{1 + k_m l_{ls}}\frac{i_r^2}{i_{dr}^e}\right]\left(\hat{k}_m - k_m\right) \quad (26)$$

$$\hat{i}_{dr}^e - \tilde{i}_{dr}^e = \frac{\lambda_s}{l_s}\left[1 + \frac{l_{ls} i_{dr}^e}{\lambda_s}\left(\frac{i_r}{i_{dr}^e}\right)^2\right]\left(1 - \frac{\hat{k}_m}{k_m}\right) \quad (27)$$

Obviously as $\hat{k}_m \to k_m$, $\hat{i}_{dr}^e - \tilde{i}_{dr}^e \to 0$

Therefore, the following block diagram of the estimator as shown in Fig.4 (a) is proposed. Fig.4 (b) shows the small signal model of the above estimator. The estimator is stable for all values of $i_{dr}^e > 0$. Also, the bandwidth of the estimator is limited only by noise consideration.

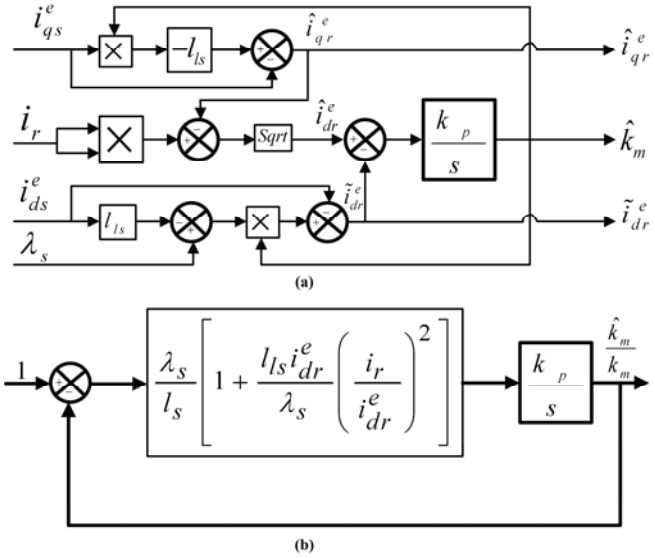

Fig.4. l_m estimator, (a) block diagram (b) small signal model.

A similar model may be developed for the reactive power based MRAS observer for slip frequency shown in Fig.3. Q_{ref} as defined in equation (13) is reference frame independent. Therefore, one can write the expression of Q_{ref} in the stator flux oriented reference frame as

$$Q_{ref} = v^e_{qr} i^e_{dr} - v^e_{dr} i^e_{qr} \tag{28}$$

Substituting the expression for v^e_{qr} & v^e_{dr} from equations (11) & (12)

$$Q_{ref} = \omega_{sl}\left(\lambda^e_{dr} i^e_{dr} + \lambda^e_{qr} i^e_{qr}\right) - \left(i^e_{qr}\, p\lambda^e_{dr} - i^e_{dr}\, p\lambda^e_{qr}\right) \tag{29}$$

Now $\lambda^e_{dr} = \sigma l_r i^e_{dr} + \dfrac{l_m}{ls}\lambda_s, \qquad \lambda^e_{qr} = \sigma l_r i^e_{qr}$ (30)

$$\therefore Q_{ref} = \omega_{sl}\left(\sigma l_r i_r^2 + \frac{l_m}{ls}\lambda_s i^e_{dr}\right) + \sigma l_r\left(i^e_{dr}\, p i^e_{qr} - i^e_{qr}\, p i^e_{dr}\right) \tag{31}$$

where $p\lambda_s = 0$ has been assumed as the machine normally operates at constant stator flux . $\dfrac{l_m}{l_s} i^e_{dr} = \dfrac{\lambda_s}{l_s} - i^e_{ds}$

$$\therefore Q_{ref} = \omega_{sl}\left(\sigma l_r i_r^2 + \frac{\lambda_s^2}{ls} - \lambda_s i^e_{ds}\right) + \sigma l_r\left(i^e_{dr}\, p i^e_{qr} - i^e_{qr}\, p i^e_{dr}\right) \tag{32}$$

$$Q_{est} = \hat{\omega}_{sl}\left(\sigma \hat{l}_r i_r^2 + \frac{\lambda_s^2}{\hat{ls}} - \lambda_s i^e_{ds}\right) \tag{33}$$

where a variable / parameter with a '^' on its top denotes its estimate. MRAS error 'ε' (defined in eqn. (16)) is given by

$$\varepsilon = Q_{ref} - Q_{est} = \lambda_s i^e_{ds}\left(\hat{\omega}_{sl} - \omega_{sl}\right) + \lambda_s^2\left(\frac{\omega_{sl}}{ls} - \frac{\hat{\omega}_{sl}}{\hat{ls}}\right) + i_r^2\left(\omega_{sl}\sigma l_r - \hat{\omega}_{sl}\sigma \hat{l}_r\right) + \sigma l_r i^{e2}_{dr}\, p\left(\frac{i^e_{qr}}{i^e_{dr}}\right) \tag{34}$$

Now making small signal assumption i.e.

$$\left(\hat{\omega}_{sl} - \omega_{sl}\right) << \omega_{sl}, \quad \left(\frac{1}{l_s} - \frac{1}{\hat{l}_s}\right) << \frac{1}{l_s} \text{ and } \left(\sigma l_r - \sigma \hat{l}_r\right) << \sigma l_r$$

$$\varepsilon = \left(\sigma l_r i_r^2 + \frac{\lambda_s^2}{ls} - \lambda_s i^e_{ds}\right)\left(\hat{\omega}_{sl} - \omega_{sl}\right) + \lambda_s^2 \omega_{sl}\left(\frac{1}{ls} - \frac{1}{\hat{ls}}\right) + i_r^2 \omega_{sl}\left(\sigma l_r - \sigma \hat{l}_r\right) + \sigma l_r i^{e2}_{dr}\, p\left(\frac{i^e_{qr}}{i^e_{dr}}\right) \tag{35}$$

Therefore, the small signal model of the slip frequency estimator of Fig.3 is given by the block diagram shown in Fig.5. If the l_m estimator described before is made much faster than ω_{sl} estimator then $\left(\dfrac{1}{ls} - \dfrac{1}{\hat{ls}}\right)$ and $\left(\sigma l_r - \sigma \hat{l}_r\right) \approx 0$. This can be ensured by incorporating an additional first order lag in the ω_{sl} estimator as shown in the block diagram below. This filter also helps to reduce the disturbance in the estimated slip frequency ($\hat{\omega}_{sl}$) due to the third disturbance input during transient conditions when $pi^e_{qr} \neq 0$ and $pi^e_{dr} \neq 0$.

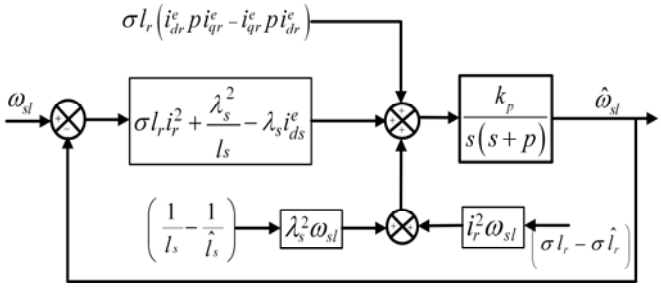

Fig.5. Small signal model of ω_{sl} estimator.

V. EXPERIMENTAL AND SIMULATION VERIFICATION OF THE Q-MRAS BASED SENSORLESS CONTROL ALGORITHM

The stand-alone VSCF generator along with the proposed sensorless controller was simulated in MATLAB/SIMULINK as well as verified on an experimental prototype. The specifications and electrical parameters of the induction machine are given in TABLE I. The controller and estimator parameters are given in TABLE II. The block diagram of the laboratory proto type VSCF generator is shown in Fig.6. Specifications of the power circuit elements and the controller gains are the same as in TABLE I and TABLE II respectively. The Q-MRAS based sensorless control algorithm is implemented using RT-LAB real-time simulation platform from Opal-RT. The prime mover for the laboratory tests is a voltage controlled dc shunt motor. An incremental encoder is also mounted on the DFIG shaft. However, the speed information is used only to compare the actual speed with the estimated speed and not used by the controller.

TABLE I
SPECIFICATIONS OF THE SYSTEM

Induction Machine (Stator referred)	
Stator (8 pole, ∇ connected)	220 V, 50 Hz, 22 A (RMS)
Rotor (8 pole, Y connected)	300V, 9A(RMS)
Rated power	5.6kW
Rated speed	720 RPM
Stator resistance/ phase (r_s)	0.87 Ω
Rotor resistance/ phase (r'_r)	1.12 Ω
Stator reactance/ phase (x_l)	12.4 Ω
Rotor reactance/ phase (x'_l)	12.4 Ω
Magnetizing reactance/ phase (x_m)	11.3 Ω
Converter rating	
Stator side: 230V(RMS), 12A (RMS)	Rotor side: 230V (RMS), 9A(RMS)
Filter Parameters	
Inductor(l_f) : 1.36 mH,30A ESR (r_f) : 0.1Ω	Capacitor(c_f) : 35μF,450V, Δ connected

TABLE II
CONTROLLER PARAMETERS

Controller Parameters		
Filter current controllers (i^e_{qf}, i^e_{df})	K_p=15 Ohm	K_i=300 (Farad)$^{-1}$
Stator voltage controllers (v^e_{qs}, v^e_{ds})	K_p=0.20 Mho	K_i=2 (Henry)$^{-1}$
Rotor current controllers (i^e_{qr}, i^e_{dr})	K_p=30 Ohm	K_i=6000 (Farad)$^{-1}$
DC link voltage controller (V_{dc})	K_p=1 Mho	K_i=1 (Henry)$^{-1}$
Stator flux controller (λ_s)	K_p=600 (s)$^{-1}$	K_i=24000 (s)$^{-2}$
Estimator Parameters		
Mutual inductance (l_m) estimator	K_p=10000 (Coulomb)$^{-1}$	
Slip frequency (ω_{sl}) estimator	K_p=70000 Joule^{-1}.s^{-2}	P =700 rad/s

The proposed Q-MRAS based sensorless control algorithm was tested (both by simulation and experiment) under different operating conditions such as DC link voltage build-up, acceleration/ deceleration of the prime mover, load transient, rotor d-axis current transient, nonlinear and unbalanced loading. The test results along with discussions are presented in this section. Fig. 7 (a) shows that this Q-MRAS speed estimator output ($\hat{\omega}_r$) starts from an initial value of zero and converges to the actual speed after a brief transient during the DC link build-up phase. It is observed from Fig. 7(b) and (c) that the DC link voltage takes longer time to build up in the experiment compared to simulation. This can be explained from the fact that the machine iron loss and the converter losses are not modeled in simulation. Therefore, with the same I_{qre} (hence same mechanical power input to the system) the power available for DC link capacitor charging is more in the simulation model allowing it to charge faster. Due to the same reason I_{qre} settles to a higher value in steady state after the DC link voltage build up phase in the experimental proto type.

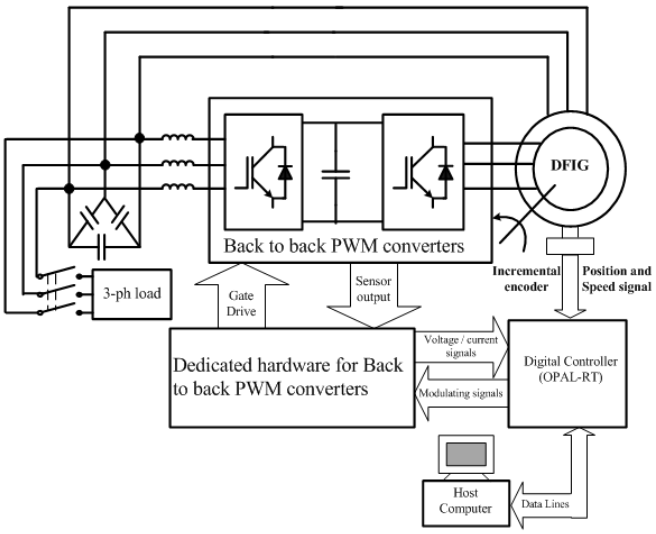

Fig.6. Block diagram of the proto type VSCF generator.

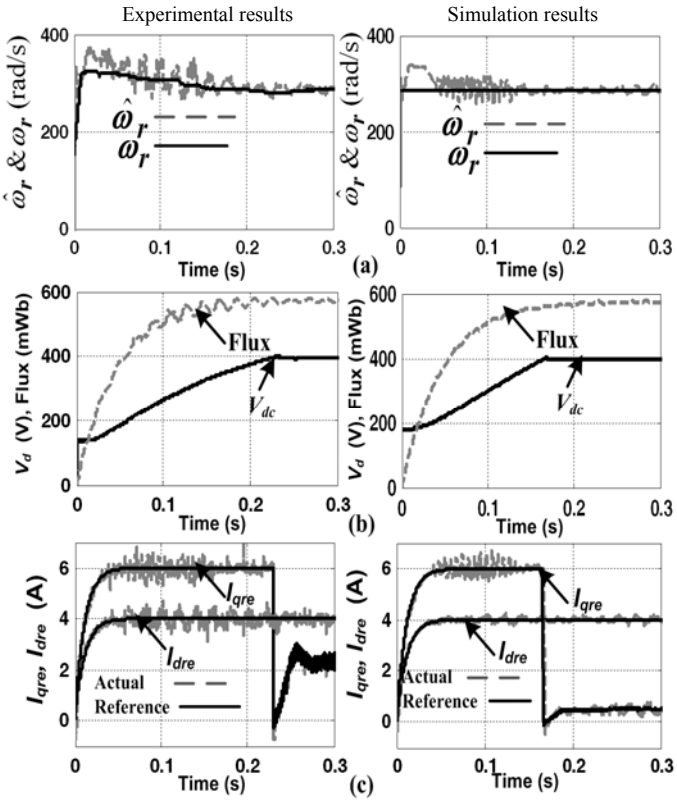

Fig.7. Experimental and simulation results of Q-MRAS during DC link voltage build up at sub-synchronous speed (a) Actual and estimated rotor speed, (b) Stator flux and DC link voltage, (c) q^e-d^e-axis actual and reference rotor currents.

The waveforms are shown for sub synchronous operation (680 RPM) of the generator. Similar results were obtained at super synchronous speed.

After the DC link build up phase, the load demand is increased to 2.8 kW (50 % of the rated machine power) in a single step. Fig.8. (a) shows estimated and actual machine speed as well as the load RMS voltage during this load transient condition. There is no significant change in the load RMS voltage although I_{qre} (Fig.8. (b)) increases substantially to increase mechanical power capture. For comparison the time scale of the experimental waveforms have been expanded during some transient periods. The experimental waveform of I_{qre} shows slightly less overshoot compared to the simulation waveform since the initial speed of the experimental setup (and hence mechanical power input/amp of I_{qre}) was higher as seen from Fig. 8(a). However, as the steady state speed in both cases are the same, due to the reasons stated in connection with Fig. 7(c), the steady state value of I_{qre} in the experiment is higher compared to simulation. To test the effect of change in the direct axis rotor current command $I_{dr}^{'*}$ is increased from 4A to 6A first, decreased from 6A to 2A next and again brought back to 4A. The load voltage remains unchanged during this variation (Fig. 8.(a)). I_{qre} also remains almost constant during $I_{dr}^{'*}$ transient (Fig. 8. (b)), indicating correct stator flux orientation. The estimated value of l_m remains essentially constant in simulation since machine saturation was not modeled. In the laboratory prototype however, estimated value of l_m shows noticeable variation during I_{dre} transient. When i_{dr}^e increases, in order to maintain constant stator flux (λ_s), i_{ds}^e decreases. Therefore, *d*-axis component of the air gap flux $\lambda_{dm}^e = \lambda_s - l_{ls} i_{ds}^e$ increases causing higher degree of machine saturation. Therefore, l_m decreases. This is correctly estimated as shown in Fig. 8(c). The reverse situation occurs during i_{dr}^e decrease.

Fig.9 shows experimental and simulation results when the prime mover speed is changed from 420 rad/s (1003 RPM) to 282 rad/s (674 RPM) and back in 0.8 sec (both in simulation and in experiment) with the generator lightly loaded. The estimated and measured speed shows good match (Fig. 9(a)). From this figure (and Fig.7 (a)) it can be concluded that the proposed Q-MRAS estimator works satisfactorily for all the operating modes of the system including DC link voltage build up phase. The rotor current makes smooth transition through the synchronous speed (Fig. 9 (c)). The prime mover speed variation has no effect on the DC link or load RMS voltage (Fig. 9 (b)).

In order to verify the harmonic compensation performance of the stator voltage controller, a 4.4 kW (78.5 % of m/c rating) balanced 3 phase nonlinear (diode rectifier feeding a resistive load on the dc side) load is applied in a single step. The experimental waveforms and the Discrete Fourier Transform (DFT) of the nonlinear load current, load voltage and stator current are shown in Fig.10. (a)-(f). The load voltage is found to remain constant with negligible distortion.

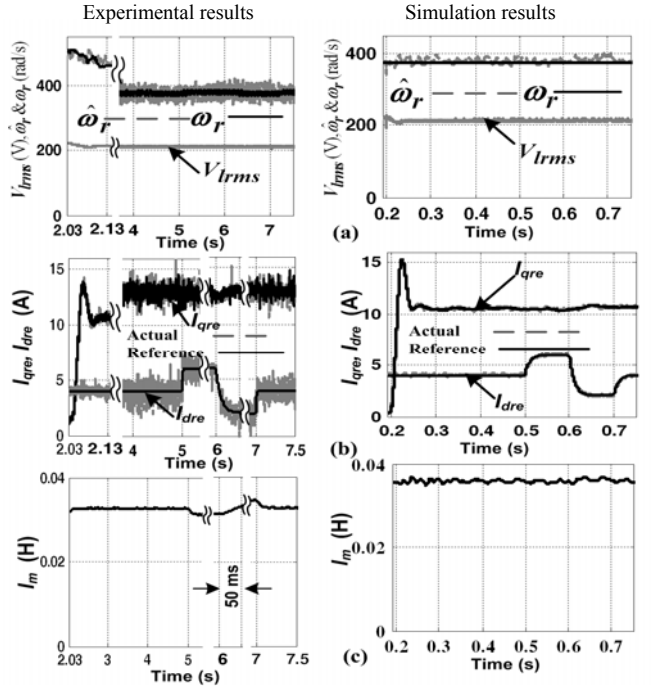

Fig.8. Experimental and simulation results of Q-MRAS during load and I_{dre} transient condition (a) Actual and estimated rotor speed and RMS load voltage, (b) q^e-d^e-axis actual and reference rotor currents (c) Estimated l_m.

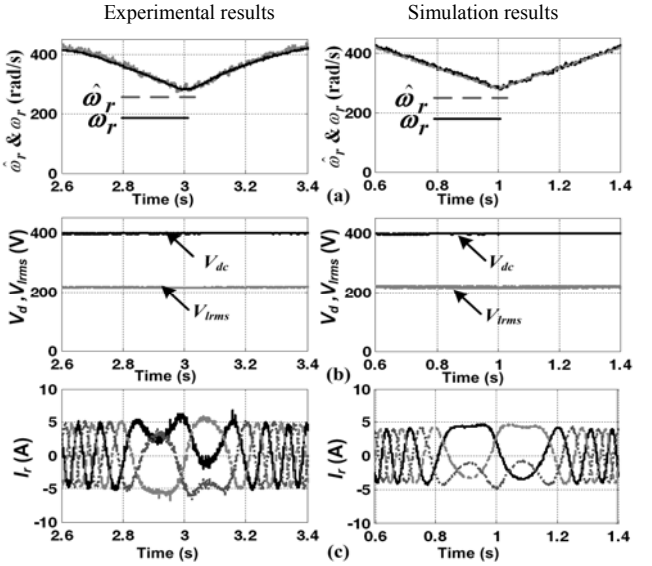

Fig.9. Experimental and simulation results of Q-MRAS during speed transient (a) Actual and estimated rotor speed (b) DC link voltage and RMS load voltage, (c) rotor currents.

The Total Harmonic Distortion (THD) of the load voltage is 2.4 % and THD of the stator current is 1.66 % while the load current THD is 27.36 %. Similar results presented in [10] shows larger load voltage THD (2.57 %) and stator current THD (6.63%) for much lower level (28 % of m/c rating) of nonlinear loading. A comparison with similar result shown in [22] shows that the proposed Q-MRAS based controller retains the excellent harmonic compensation performance of the sensor based system proposed in [22].

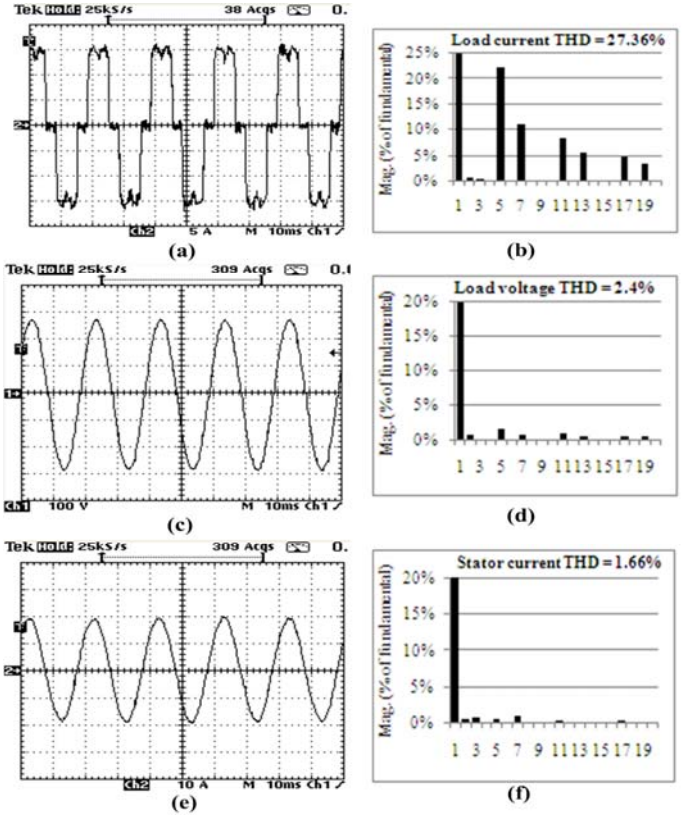

Fig.10. Experimental waveforms with 3-ph nonlinear load (a) Load Current,(b) DFT of the load current, (c) load Voltage (d) DFT of the load voltage (e) stator current (f) DFT of the stator current.

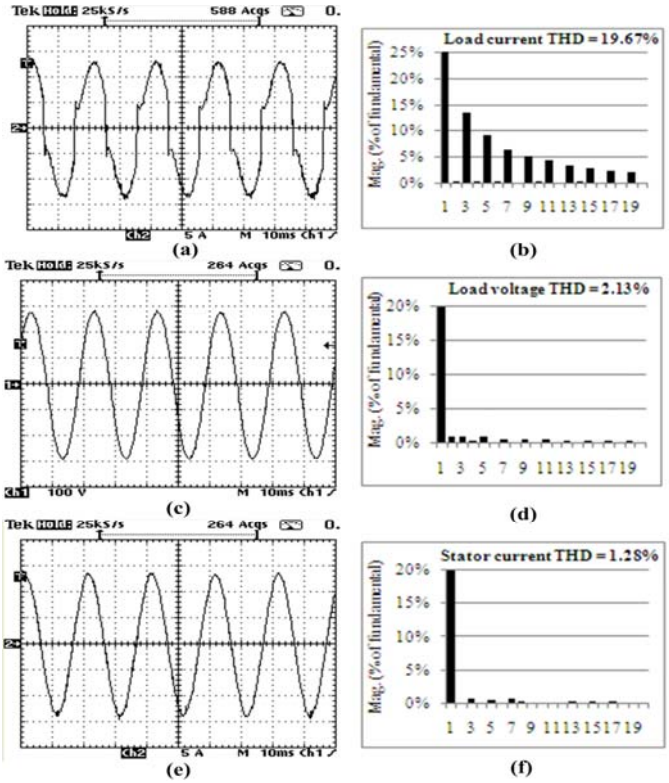

Fig.11. Experimental waveforms with 1-ph nonlinear load (a) Load current, (b) DFT of the load current, (c) load voltage, (d) DFT of the load voltage, (e) stator current, (f) DFT of the stator current.

Next the system is tested with an unbalanced nonlinear load, in the form of a single phase diode rectifier feeding a RL-load. This single phase nonlinear load of 2.1 kW (37.5 % of m/c rating) is connected between two lines in a single step. The experimental waveforms and the DFT of the unbalanced nonlinear load current, load voltage and stator current are shown in Fig.11. (a)-(f) respectively. To the best of our knowledge, performance of speed sensorless stand-alone DFIG based VSCF systems with this type of load (i.e. unbalanced nonlinear) has not been reported in the literature so far. Hence no comparison could be made. The THD and the negative sequence component of the load line voltage and stator current obtained from both simulation and experiment is compared in TABLE III. Finally Fig.12 shows the Q-MRAS based speed estimator performance during balanced and unbalanced nonlinear loading. It is observed that even with such large nonlinear/ unbalanced load the estimator performs satisfactorily.

TABLE III
PERFORMANCE COMPARISION

	Simulation results	Experimental results
Load current THD (3-ph-nonlinear , 4.4kW)	26.65 %	27.36 %
Load line voltage THD (3-ph-nonlinear, 4.4kW)	2.25 %	2.4 %
Stator current THD (3-ph-nonlinear, 4.4kW)	0.92 %	1.66 %
Load current THD (1-ph-nonlinear, 2.1kW)	19.46 %	19.67 %
Load line voltage THD (1-ph-nonlinear, 2.1kW)	1.15 %	2.13 %
Stator current THD (1-ph-nonlinear, 2.1kW)	0.86 %	1.28 %
Negative sequence component of stator voltage (1-ph-nonlinea, 2.1kW)	0.65 %	1.65 %
Negative sequence component of stator current (1-ph-nonlinear, 2.1kW)	0.65 %	1.48 %

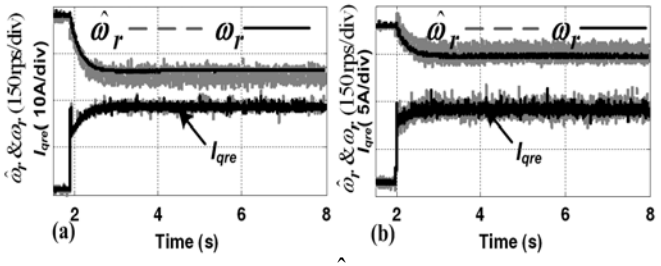

Fig.12. Experimental waveforms of $\hat{\omega}_r$ & ω_r and I_{qre} (a) with 4.4 kW 3-ph nonlinear load, (b) with 2.1 kW 1-ph nonlinear load current.

VI. CONCLUSION

This paper has presented a sensorless control strategy based on reactive power driven Model Reference Adaptive System for a DFIG based stand-alone VSCF generator. The proposed algorithm is suitable for all operating modes of the generator including the start up DC link build up phase, thus completely eliminating the speed sensor. It also maintains correct field orientation during load (nonlinear and unbalanced) transients and exhibits improved load voltage regulation property compared to available literature. Even with large nonlinear (up

to 78.5 % of the machine rating) and unbalanced load (up to 37.5 % of the machine rating) the load voltage unbalance and harmonic distortions are negligible. Unlike previously reported methods of harmonic and unbalanced current compensation, in such systems the control strategy proposed in this paper does not adversely affect the machine operation by producing additional harmonic heating or pulsating torque. Most importantly, the algorithm ensures little degradation in the load voltage quality even when supplying loads which are unbalanced as well as nonlinear. To the best of our knowledge no such system has been reported in the literature so far. The proposed system, therefore, meets the dual requirement of a stand-alone generator of reduced maintenance (by eliminating speed sensor) and improved power quality while supplying unbalanced and nonlinear loads.

REFERENCES

[1] R. Pena, J. C. Clare, and G. M. Asher, "Doubly fed induction generator using back-to-back PWM converters and its application to variable speed wind-energy generation," *IEE Proc. Elect. Power Appl,* vol. 143, no. 3, pp. 231-241, May 1996.

[2] R. Datta and V. T. Ranganathan, "A simple position-sensorless algorithm for rotor-side field-oriented control of wound-rotor induction machine," *IEEE Trans. Ind. Electron.,* vol. 48, no.4, pp. 786-793, Aug. 2001.

[3] A. C. Smith, R. Todd, M. Barnes, and P. J. Tavner, "Improved energy conversion for doubly fed wind generators," *IEEE Trans. Ind. Appl.,* vol. 42, no.6, pp. 1421-1428, Nov. 2006.

[4] Y. Jun, L. Hui, L. Yong, and C. Zhe, "An improved control strategy of limiting the DC-Link voltage fluctuation for a doubly fed induction wind generator," *IEEE Trans. Power Electron.,* vol. 23, no.3, pp. 1205-1213, May 2008.

[5] R. Pena, J. C. Clare, and G. M. Asher, "A doubly fed induction generator using back-to back PWM converters supplying an isolated load from a variable speed wind turbine," *IEE Proc. Elect. Power Appl.*, vol. 143, no. 5, pp. 380-387, Sept. 1996.

[6] R. Cardenas, R. Pena, J. Proboste, G. Asher, and J. Clare, "MRAS observer for sensorless control of standalone doubly fed induction generators," *IEEE Trans. Energy Convers.,* vol. 20, no. 4, pp. 710-718, Dec. 2005.

[7] R. Cardenas, R. Pena, J. Clare, G. Asher, and J. Proboste, "MRAS observers for sensorless control of doubly-fed induction generators," *IEEE Trans. Power Electron.,* vol. 23, no.3, pp. 1075-1084, May 2008.

[8] G. Iwanski and W. Koczara, "Sensorless direct voltage control of the stand-Alone slip-ring induction generator," *IEEE Trans. Ind. Electron.,* vol. 54, no.2, pp. 1237-1239, Apr. 2007.

[9] G. Iwanski and W. Koczara, "DFIG based power generation system with UPS function for variable speed application," *IEEE Trans. Ind. Electron.,* vol.55, no. 8, pp. 3047-3054, Aug. 2008.

[10] A. K. Jain and V. T. Ranganathan, "Wound rotor induction generator with sensorless control and integrated active filter for feeding nonlinear loads in a stand-alone grid," *IEEE Trans. Ind. Electron.,* vol. 55, no.1, pp. 218-228, Jan. 2008.

[11] R. Pena, R. Cardenas, E. Escobar, J. Clare, P. Wheeler, "Control strategy for a doubly-fed induction generator feeding an unbalanced grid or stand-alone load," *Electr. Power Syst. Res.,* Vol. 79, no. 2, pp. 355-364, Feb. 2009.

[12] T. Bhattacharya and L. Umanand, "Rotor position estimator for stator flux-oriented sensorless control of slip ring induction machine," *IET Elect. Power Appl.,* vol. 3, no.1, pp. 67-76, Jan. 2009.

[13] G. D. Marques, V. F. Pires, S. Sousa, and D. M. Sousa, "A DFIG sensorless rotor-position detector based on a hysteresis controller," *IEEE Trans. Energy Convers.,* vol. 26, pp. 9-17, Mar. 2011.

[14] G. D. Marques and D. M. Sousa, "Air-gap-power-vector-based sensorless method for DFIG control without flux estimator," *IEEE Trans. Ind. Electron.,* vol. 58, no.10, pp. 4717-4726, Oct. 2011.

[15] G. D. Marques and D. M. Sousa, "New sensorless rotor position estimator of a DFIG based on torque calculations—stability study," *IEEE Trans. Energy Convers.,* vol. 27, no.1, pp. 196-203, Mar. 2012.

[16] V.-T. Phan and H.-H. Lee, "Improved predictive current control for unbalanced stand-alone doubly-fed induction generator-based wind power systems," *IET Electr. Power Appl.,* vol. 5, no.3, pp. 275-287, Mar. 2011.

[17] V.-T. Phan and H.-H. Lee, "Stationary frame control scheme for a stand-alone doubly fed induction generator system with effective harmonic voltages rejection," *IET Electr. Power Appl.,* vol. 5, no.9, pp. 697-707, Nov. 2011.

[18] P. Van-Tung and L. Hong-Hee, "Control strategy for harmonic elimination in stand-alone DFIG applications with nonlinear loads," *IEEE Trans. Power Electron.,* vol. 26, no.9, pp. 2662-2675, Sept. 2011.

[19] S. Maiti and C. Chakraborty, "MRAS-based speed estimation techniques for vector controlled double inverter-fed slip ring induction motor drive," *IECON 2008, IEEE 34th Annual Conference*, pp. 1275-1280, Nov. 2008.

[20] V.Verma, S.Maiti and C.Chakraborty, "Grid-connected vector-controlled slip-ring induction motor drive without speed sensor," *Simul. Modell. Pract. Theory,* vol.18, no.7, pp.984-997, Aug. 2010.

[21] M. Pattnaik and D. Kastha, "Comparison of MRAS based speed estimation methods for a stand-alone doubly fed induction generator," *ICEAS-2011*, *ITER* Bhubaneswar, India, pp.1-6, Dec. 2011.

[22] M. Pattnaik and D. Kastha, "Control of double output induction machine based stand-alone variable speed constant frequency generator with nonlinear and unbalanced loads," *IEEE PES General Meeting 2010*, Minneapolis, Minnesota, USA, pp.1-8, Jul. 2010.

[23] M. Pattnaik and D. Kastha, "Reactive power based MRAS observer for speed sensorless control of double output induction generator," *ICIIS 2010,* NIT Surathkal, India, pp.556-561, Jul./Aug. 2010.

BIOGRAPHIES

Monalisa Pattnaik (S'11) received the B.Tech. degree in Electrical Engineering from College of Engineering and Technology, OUAT, Bhubaneswar, Orissa, India, in 1999 and the M. Tech. degree in Machine Drives and Power Electronics from Indian Institute of Technology Kharagpur, India, in 2006 and she is pursuing the Ph.D. degree at Indian Institute of Technology, Kharagpur. She was working in the department of Electrical Engineering, Institute of Technical Education and Research, SOAU, Bhubaneswar, Odisha from June 2002 to July 2008. Now she has joined as an Asst. Professor in the department of Electrical Engineering, NIT Rourkela, Odisha, India. Her research area is Machine Drives and Power Electronics.

Debaprasad Kastha (M'94) received the B.E. degree in Electrical Engineering from Bengal Engineering College, Calcutta University, India, in 1987, the M.E. degree in electrical engineering from Indian Institute of Science, Bangalore in 1989 and the Ph.D. degree from the University of Tennessee, Knoxville, in 1994.

From March 1989 to December 1989 he worked in the Research and Development (Electronics) Division, Crompton Greaves, Ltd, Bombay, India. He joined the Department of Electrical Engineering, Indian Institute of Technology, Kharagpur, India as a lecturer in April 1994, became Asst. Professor in Jan. 1996. Presently he holds the post of Professor. His research interest includes Wind Energy, Machine Drives and Power Electronics.